Polymer Chemistry

ROYAL SOCIETY OF CHEMISTRY

PAPER

View Article Online
View Journal | View Issue

Check for updates

Cite this: *Polym. Chem.*, 2025, **16**, 1162

Poly(β-hydroxyalkanoate)/polymethacrylate self-assembled architectures by ring-opening polymerization (ROP)/reversible addition–fragmentation chain-transfer (RAFT) polymerization and polymerization-induced self-assembly (PISA)†

Julien Rosselgong,* Ali Dhaini, Manon Rochedy, Lourdes Mónica Bravo-Anaya, Jean-François Carpentier and Sophie M. Guillaume*

Self-assembled poly(β-hydroxyalkanoate) (PHA)-based block copolymers are attractive materials for biomedical applications due to the biocompatibility and (bio)degradability of the PHA segment. Herein, we report the synthesis and formation of self-assemblies based on PHAs: namely, poly(3-hydroxybutyrate) (PHB) was prepared by ring-opening polymerization (ROP) of racemic β-butyrolactone (*rac*-β-BL) using a discrete yttrium-based catalyst in the presence of a hydroxy-terminated trithiocarbonate (TTC-OH) as initiator. The resulting TTC end-capped PHB prepolymer next promoted the controlled reversible addition–fragmentation chain-transfer (RAFT) polymerization of 2-hydroxy ethyl methacrylate (HEMA). When performed in THF, in which the initial solvophilic PHB-TTC segment and HEMA monomer are both fully soluble, this second step resulted in a polymerization-induced self-assembly (PISA) leading to the formation of nanoparticles, as the solvophobic PHEMA precipitated in the dispersed medium. The effective extension of the PHB block by a PHEMA segment, as evidenced by SEC and NMR analyses, highlighted the efficiency of the PHB-TTC macro-RAFT agent. This ROP/RAFT/PISA strategy revealed successful at various polyester (DP = 45–90) and polymethacrylate (DP = 200–500) block lengths. The size, polydispersity index (PDI) and morphology of the resulting self-assembled PHB$_x$-*b*-PHEMA$_y$ particles were assessed by dynamic light scattering (DLS) measurements, transmission electron microscopy (TEM) and small-angle X-ray scattering (SAXS). Depending on both segments chain-lengths, DLS enabled identifying particles in suspension having hydrodynamic diameters (D_H) varying from 56 to 194 nm, with narrow polydispersity index, *i.e.* PDI < 0.140. SAXS measurements and TEM observations revealed vesicles morphology for specific PHB$_x$-*b*-PHEMA$_y$ samples presenting apparent diameters ranging from 134 to 316 nm. These morphologies support the successful copolymerization through a PISA process, first reported herein for the elaboration of PHA-based objects that may be valuable nano-vehicles of active ingredients for biomedical applications.

Received 17th December 2024,
Accepted 27th January 2025

DOI: 10.1039/d4py01447b

rsc.li/polymers

Introduction

Polyhydroxyalkanoate (PHA)-based block copolymers are valuable polyester materials for applications in nanomedicine and/or drug delivery.[1–8] While PHAs are most commonly associated with other polyesters (typically another PHA or poly(ethylene glycol)), growing a second poly(meth)acrylic block from a PHA segment by reversible-deactivation radical polymerization (RDRP) is less documented.[9–11] For more than two decades, RDRP techniques such as nitroxide-mediated polymerization (NMP), atom transfer radical polymerization (ATRP) or reversible addition–fragmentation chain-transfer (RAFT) polymerization have revealed key synthetic tools to access well-defined (co)polymers, including block copolymers.[12–15] For instance, poly((*R*)-3-hydroxybutyrate) (PHB)-based triblock copolymers poly((*R*)-3-hydroxybutyrate)-*b*-poly(*N*-isopropylacrylamide)-*b*-[[poly(methyl ether methacrylate)-*g*-poly(ethylene glycol)]-*co*-[poly(methacrylate)-*g*-poly(propylene glycol)]], a multi-arm star copolymer providing a thermo-responsive hydro-

Univ. Rennes, CNRS, Institut des Sciences Chimiques de Rennes, UMR 6226, 35042 Rennes, France. E-mail: julien.rosselgong@univ-rennes.fr, sophie.guillaume@univ-rennes.fr

† Electronic supplementary information (ESI) available. See DOI: https://doi.org/10.1039/d4py01447b

gel, was prepared by ATRP for thermogels outcomes.[16] The double thermo-responsive behavior due to the (meth)acrylate blocks enabled the copolymer self-assembly at room temperature, and the subsequent delivery of a drug at body temperature. Also, RAFT enabled preparing novel PHB macro-RAFT agents subsequently used to grow an *N*-isopropyl acryl amide (NIPAM) segment, ultimately offering thermo-responsive block copolymers.[17] In this latter example, the macro-RAFT agent was synthesized in two steps from esterification of an ω-hydroxylated PHB - first made by ring-opening polymerization (ROP) of racemic β-butyrolactone (*rac*-β-BL) with a RAFT agent, namely 2-(dodecylthiocarbonothioylthio)-2-methylpropionic acid used as initiator combined with a yttrium catalyst-, using 4-dimethylaminopyridine (DMAP) and *N*,*N*′-dicyclohexylcarbodiimide (DCC) as coupling agents.

Growing *in situ* a hydrophobic chain from a soluble first-block to recover an amphiphilic block copolymer, is a process referred to as polymerization-induced self-assembly (PISA). Provided a formulation including a soluble polymer segment is chain-extended using a monomer of which the corresponding homopolymer is insoluble in the reaction solvent, PISA results in nano-objects such as micelles, worms and/or vesicles.[18–23] In this process, the growing second-block becomes insoluble when reaching a critical degree of polymerization (DP), eventually leading to an *in situ* self-assembly phenomenon. Such systems are essentially based on non-solvents such as water,[24–31] alcohols,[32–36] or non-polar solvents.[37–41] While a wide variety of PISA formulations have been established, to our knowledge, there is no report of PISA involving a PHA polyester block.

Recently, aqueous ROP and PISA were successfully combined to form *N*-carboxyanhydrides (NCAs)-based copolymers by ROPISA, as reported by Bonduelle and co-workers.[42,43] An α-amino end-capped poly(ethylene oxide) macroinitiator was used in order to protect the NCA monomers from hydrolysis during their ROP performed in water. The spontaneous self-assembly of the amphiphilic poly(ethylene oxide)/polypeptide block copolymers thus led to a PISA formulation returning needle-like nanoparticles. Such a NCA ROPISA approach was further investigated by Thornton and co-workers using a polysarcosine macroinitiator to form only poly(amino acid)-based (L-phenylalanine-NCA and alanine-NCA) rod-like nanoparticles, and also by Heise and co-workers to access amino acid-based (L-proline-NCA) worm like micelles nanostructures loaded with dyes.[44,45]

More recently, Armes and coworkers reported the efficient synthesis of hydrolytically degradable block copolymer nanoparticles by reverse PISA in aqueous media.[46] A poly(ε-caprolactone) (PCL)-based macroinitiator and a suitable water-miscible monomer (*N*,*N*′-dimethylacrylamide, DMAC) afforded PCL-*b*-PDMAC and PDMAC-*b*-PCL-*b*-PDMAC diblock and triblock copolymers, respectively. These copolymers were insoluble in water, thus leading to the formation of polyester/polyacrylamide micelles with sizes ranging from 20 to 120 nm. Later on, the same authors combined PISA with crystallization-driven self-assembly to form anisotropic nanoparticles from poly(L-lactide)-*b*-PDMAC copolymers. They obtained either rod-like nanoparticles or diamond-like platelets that have potential applications as sustainable pickering emulsifiers.[47] Further on, the same group reported the RAFT dispersion polymerization of 2-hydroxyethyl methacrylate in non-polar media.[48] Using a poly(lauryl methacrylate) (PLMA) precursor, a PISA process then generated PLMA-PHEMA nanoparticles forming well-defined nearly monodispersed spheres.

Herein, we report the formation of PHB-based self-assembled architectures through a combined ROP, RAFT and PISA process. As inspired by our previous work on the yttrium catalyzed ROP of β-lactones performed in the presence of an exocyclic alcoholic initiator, the ROP of racemic β-BL catalyzed by a discrete yttrium complex, in the presence of a RAFT agent acting as an alcohol moiety, afforded the PHB prepolymer that subsequently promoted the RAFT of 2-hydroxyethyl methacrylate (HEMA) by dispersion PISA performed in THF.[49,50] The PHB block length and the degree of polymerization (DP) of the second PHEMA segment of the resulting PHB-*b*-PHEMA nano-objects, were assessed by size exclusion chromatography (SEC). Particle size and morphology were determined using dynamic light scattering (DLS) measurements, transmission electron microscopy (TEM) and small-angle X-ray scattering (SAXS) analyses. The corresponding pseudo-phase diagram established by DLS revealed an increase of the hydrodynamic diameter (D_H) of particles formed with the increase of the DP of the HEMA second block and with the initial co-monomer and PHB macro-RAFT agent concentration. These results thus established a PISA process applied for the first time to elaborate PHA/polymethacrylate objects.

Experimental section

Materials and methods

All experiments involving organometallic catalysts were performed under an inert atmosphere (argon, <5 ppm O_2 and H_2O) using standard Schlenk, vacuum line, and glovebox techniques. Racemic β-butyrolactone (*rac*-β-BL) (>95%, Aldrich) was distilled twice from CaH_2 prior to use. 2-Hydroxyethyl methacrylate (HEMA) (>99%, Aldrich; containing traces of ethylene glycol dimethacrylate cross-linker as established by GC-MS analyses, Fig. S1†)[51] was purified prior to use, upon passing it through a basic alumina column to remove the monomethyl ether hydroquinone inhibitor. The RAFT chain transfer agent (CTA) 4-cyano-4-[(dodecylsulfanylthiocarbonyl)sulfanyl]pentanol (97%, Aldrich, trithiocarbonate (TTC), TTC-OH) was dried under vacuum at 60 °C prior to use. 2,2′-Azobis(2-methylpropionitrile) (AIBN, >98%, Aldrich) was used as received. The $\{ONNO^{Me^2}\}H_2$ proligand and $Y[N(SiHMe_2)_2]_3(THF)_2$ metallic precursor, from which the discrete amido yttrium complex was prepared *in situ*, were synthesized according to the reported procedure.[50] THF and toluene were freshly distilled from Na-benzophenone under argon and degassed thoroughly by freeze–thaw-vacuum cycles prior to use. All other reagents were used as received.

Instrumentation and measurements

^{1}H (500 and 400 MHz), ^{13}C{^{1}H} (125 and 100 MHz) and 2D (COSY, HMBC, HSQC, and DOSY) NMR spectra were recorded on Bruker Avance AM 500 or Ascend 400 spectrometers at 25 °C. ^{1}H and ^{13}C{^{1}H} NMR spectra were referenced internally relative to $SiMe_4$ (δ 0 ppm) using the residual solvent resonances. The analyses were recorded in $CDCl_3$ for the PHB-TTC macro-RAFT agent and in DMSO-d_6 for the PHB-*b*-PHEMA diblock copolymers.

Number-average molar mass ($M_{n,SEC}$), weight-average molar mass ($M_{w,SEC}$) and dispersity ($Đ_M = M_w/M_n$) values of the copolymers were determined by size exclusion chromatography (SEC) in THF at 20 °C for the PHB homopolymers, or in *N*,*N*-dimethylformamide (DMF + LiBr 1.0 g L^{-1}) at 20 °C for the PHB-*b*-PHEMA diblock copolymers. SEC in THF was stabilized with BHT at 30 °C (flow rate = 1.0 mL min^{-1}) on an Agilent 1260 Infinity II system equipped with a refractive index detector (dRI), a photo-diode array detector (DAD) and a set of two ResiPore (300 × 7.5 mm) columns. Polymer samples of PHB-TTC were dissolved in THF (1.0 mg mL^{-1}). All elution curves were calibrated with polystyrene standards (Agilent Easivial kit of polystyrene standards; M_n from 162 to 364 000 g mol^{-1}). The $M_{n,SEC}$ values of the PHBs were not corrected for the difference in hydrodynamic radius *vs.* those of polystyrene. SEC measurements in DMF were performed on an Ultimate 3000 system from Thermoscientific equipped with a DAD. The system also includes a multi-angle light scattering detector (MALS with 8 angles) and a dRI, both from Wyatt technology. Polymer samples of PHB-*b*-PHEMA were dissolved in DMF (1.0 mg mL^{-1}) and were separated with a set of three columns (GF-1G 7B (7.5 × 50 mm), GF 310 (7.5 × 300 mm) GF510 (7.5 × 300 mm); exclusion limits from 500 to 300 000 g mol^{-1}) at a flow rate of 0.5 mL min^{-1}. The columns were maintained at 50 °C. Agilent Easivial kit of polystyrene was used as standard (M_n from 162 to 364 000 g mol^{-1}). SEC DMF experiments were performed through the platform POLYCAR of the University of Bordeaux.

The molar mass of PHB samples was also determined by ^{1}H NMR analysis in $CDCl_3$ from the relative intensities of the signals of the methine hydrogen from the repeating unit (δ 5.03–5.53 ppm, –O*CH*CH_3–CH_2–C═O) and of the methylene signal of the TTC end-group (δ 3.29–3.38 ppm, *CH_2*–S–C═S). Monomer conversion was calculated from ^{1}H NMR spectra of the crude polymer samples in $CDCl_3$ by using the integration (Int.) ratios [Int.$_{PHB/PHEMA}$/(Int.$_{\beta\text{-BL/HEMA}}$ + Int.$_{PHB/PHEMA}$)] of the methine hydrogens of PHB/PHEMA (*vide supra*) and of the monomers (δ 4.32 ppm, β-BL; δ 4.17 ppm, HEMA).

High resolution (error < 25 ppm) matrix-assisted laser desorption ionization – time of flight (MALDI-ToF) mass spectrometry (MS) was performed using an ULTRAFLEX III TOF/TOF spectrometer (Bruker Daltonik Gmbh, Bremen, Germany) in positive ionization mode at the Centre Régional de Mesures Physiques de l'Ouest (CRMPO, ScanMAT UAR 2025, CNRS-Université de Rennes). MS spectra were recorded using the reflectron mode and an accelerating voltage of 25 kV. A mixture of a freshly prepared solution of the polymer in CH_2Cl_2 (HPLC grade, 10 mg.mL^{-1}) and *trans*-2-(3-(4-*tert*-butylphenyl)-2-methyl-2-propenylidene)-malononitrile (DCTB), and an acetonitrile solution of the cationizing agent (sodium trifluoroacetate, 10 mg mL^{-1}) were prepared. The solutions were combined in a ratio 1 : 1 : 1 *v*/*v*/*v* of matrix-to-sample-to-cationizing agent. The resulting solution (*ca.* 0.25–0.5 μL) was deposited onto the sample target and air or vacuum dried.

Dynamic light scattering (DLS) measurements were performed in THF using a Malvern Zetasizer NanoZS instrument equipped with a standard HeNe laser emitting at 632.8 nm (Malvern, U.K.), at 25 °C, and at an angle of 173°. The correlation functions were averaged from three independent measurements of two runs of 60 s each. The equilibration time for this measurement was 60 s. Non-negative least squares and cumulants algorithms were applied to extract the intensity-weighted particle size distribution and the intensity-weighted mean hydrodynamic size, respectively. The hydrodynamic diameter (D_H) was determined using the Stokes–Einstein equation proposed for spherical particles.[52] THF viscosity at the selected temperature was taken into account for the calculation of D_H. Measurements for each sample were at least triplicated. The size and PDI data of the objects are presented as average values along with the calculated standard deviation. Samples for DLS observations were diluted at 0.5 wt% of solids *vs.* THF.

Imaging was performed with a JEM-1400 transmission electron microscope (TEM, JEOL Ltd, Tokyo, Japan) operating at an accelerating voltage of 120 kV. Images were recorded with a Gatan SC200 Orius® CCD camera at 25 000 magnification and set up with the imaging software Gatan Digital MicrographTM (Gatan, Pleasanton, USA); images were acquired on at least three different regions. Samples for TEM observations were diluted at 0.5 wt% of solids *vs.* THF; they were prepared by direct deposition of a PHB-*b*-PHEMA suspension droplet (7 μL) on carbon grids (300 mesh Cu-300LD from Pacific Grid Tech) and THF was evaporated at room temperature over 20 min. The particle size distribution was determined one-by-one from two different TEM-micrographs using Image-J software and displayed with a standard deviation.

Small angle X-Ray Scattering (SAXS) experiments were performed on PHB_{83}-*b*-$PHEMA_{500}$ suspensions at 5 wt% and 7.5 wt% on the SWING beamline at Synchrotron SOLEIL, Gif-sur-Yvette, France. The SAXS setup included a wavelength of λ = 1.033 Å^{-1} and an energy of 12 keV, with a 17 × 17 cm^2 low-noise Aviex CCD detector positioned at distances of 0.518 and 6.136 m from the sample, yielding a *q*-range of 0.00104–2.06 Å^{-1}, where $q = 4\pi \sin\theta/\lambda$. The copolymer suspensions were placed into borosilicate capillaries (1.5 mm optical path, WJM-Glas/Müller GmbH, Germany). The intensity was collected after 1000 ms exposition (waiting gap: 2000 ms) in a vertical scan of 10 steps of 1 mm each. All 10 integrated images were averaged to obtain one $I(q)$ profile per sample. A background correction was applied on the $I(q)$ profiles by subtracting the THF scattering, and the unit was set to cm^{-1} after multiplying the measured scattering by 0.02 × 1.5/capillary diameter. The resulting data was analyzed using a spherical

vesicle model on SASView software, with the scattering length density of THF and $PHEMA_{500}$, as previously calculated, being set.

Typical procedure for the ROP of β-butyrolactone. In a typical experiment, in a glovebox, a Schlenk flask containing dried TTC-OH (201.2 mg, 516 μmol) was charged with [Y$(N(SiHMe_2)_2)_3$](THF)$_2$ (325.3 mg, 516 μmol, 1.0 equiv.) and {ONNO^{Me_2}}H$_2$ (183.9 mg, 516 μmol, 1.0 equiv.).[50] Then, toluene (3 mL) was added and the solution was stirred at room temperature (20 °C) for 10 min, followed by the rapid addition of *rac*-β-BL (4.00 g, 46.4 mmol, 90 equiv. *vs.* [Y]). The reaction mixture was stirred at 20 °C for 3 h and quenched upon air exposure. The monomer conversion was determined by ^{1}H NMR analysis in $CDCl_3$ of an aliquot of the crude mixture. After removing the volatiles under vacuum, the crude polymer was then dissolved in CH_2Cl_2 (20 mL) and precipitated three times in cold pentane, filtered and finally dried. The recovered pale yellow powder was then analyzed by ^{1}H, ^{13}C and DOSY NMR spectroscopy, MALDI-ToF mass spectrometry, and SEC analysis. ^{1}H NMR (500 MHz, $CDCl_3$, 25 °C) δ (ppm): 6.95 (m, 1H, CH_3–**CH**=CH–C=O–), 5.81 (d, J = 14 Hz, 0.2H, CH_3–CH=**CH**–C=O–), 5.24 (m, 82H, C=O–O–**CH**CH_3–CH_2–C=O), 4.18 (m, 0.6H, C=O–O–**CH**CH_3–OH), 4.12 (t, J = 5 Hz, 2H, –$CHCH_3$–CH_2-C=O–O–**C**$\mathbf{H_2}$–CH_2–), 3.32 (t, J = 8 Hz, 2H, CH_3–$(CH_2)_{10}$–**C**$\mathbf{H_2}$–S–C=S–), 2.58 (42 H, C=O–O–$CHCH_3$–C$\mathbf{H_2}$–C=O), 2.45 (42H, C=O–O–$CHCH_3$–C$\mathbf{H_2}$–C=O), 2.23 (m, 4.6 H, –S–C=S–CCNCH_3–C$\mathbf{H_2}$–), 1.87 (s, 3H, –S–C=S–CCNC$\mathbf{H_3}$–CH_2–), 1.84 (d, J = 7 Hz, 1.2H, C$\mathbf{H_3}$–CH–CH–C=O–), 1.27 (m, 249H, C=O–O–CH**C**$\mathbf{H_3}$–CH_2–C=O), 0.89 (m, 3H, **C**$\mathbf{H_3}$–$(CH_2)_{10}$–CH_2–S–C=S–) (Fig. 1). ^{13}C J-MOD NMR (125 MHz, $CDCl_3$, 25 °C) δ (ppm): 217.4 (CH_3–$(CH_2)_{10}$–CH_2–S–**C**=S–), 171.5 (S–C=S–**C**(CN)(CH_3)–CH_2–), 169.2 (C=O–O–$CHCH_3$–CH_2–**C**=O), 124.8 (CH_3–**C**H–CH–C=O–), 122.7 (CH_3–CH–**C**H–C=O–), 119.3 (S–C=S–C(**C**N)(CH_3)–CH_2–), 67.7 (C=O–O–**C**HCH$_3$–CH_2–C=O), 64.0 (S–C=S–C(CN)(**C**H$_3$)–CH_2–), 63.2 (S–C=S–C(CN)(CH_3)–CH_2–CH_2–**C**H$_2$–O), 40.7 (=O–O–$CHCH_3$–**C**H$_2$–C=O), 19.8 (C=O–O–CH**C**H$_3$–CH_2–C=O) (Fig. S2†).

Typical synthesis of PHB-*b*-PHEMA by PISA. In a typical dispersion experiment, PHB_{83}-TTC (50.0 mg, 6.66 μmol), HEMA (0.433 g, 3.33 mmol), THF (4.349 g, 90 wt% *vs.* [PHB + HEMA]) and AIBN (1.33 μmol, 2.2 μL of a 10 wt% solution in THF) were charged in a Schlenk flask preplaced in an ice bath, and degassed for 15 min with argon. The Schlenk flask was next immersed for 20 h in an oil bath preheated at 60 °C. The PHB_{83}-*b*-$PHEMA_{500}$ block copolymer obtained was then analyzed by ^{1}H NMR analysis in DMSO-d_6 of an aliquot of the

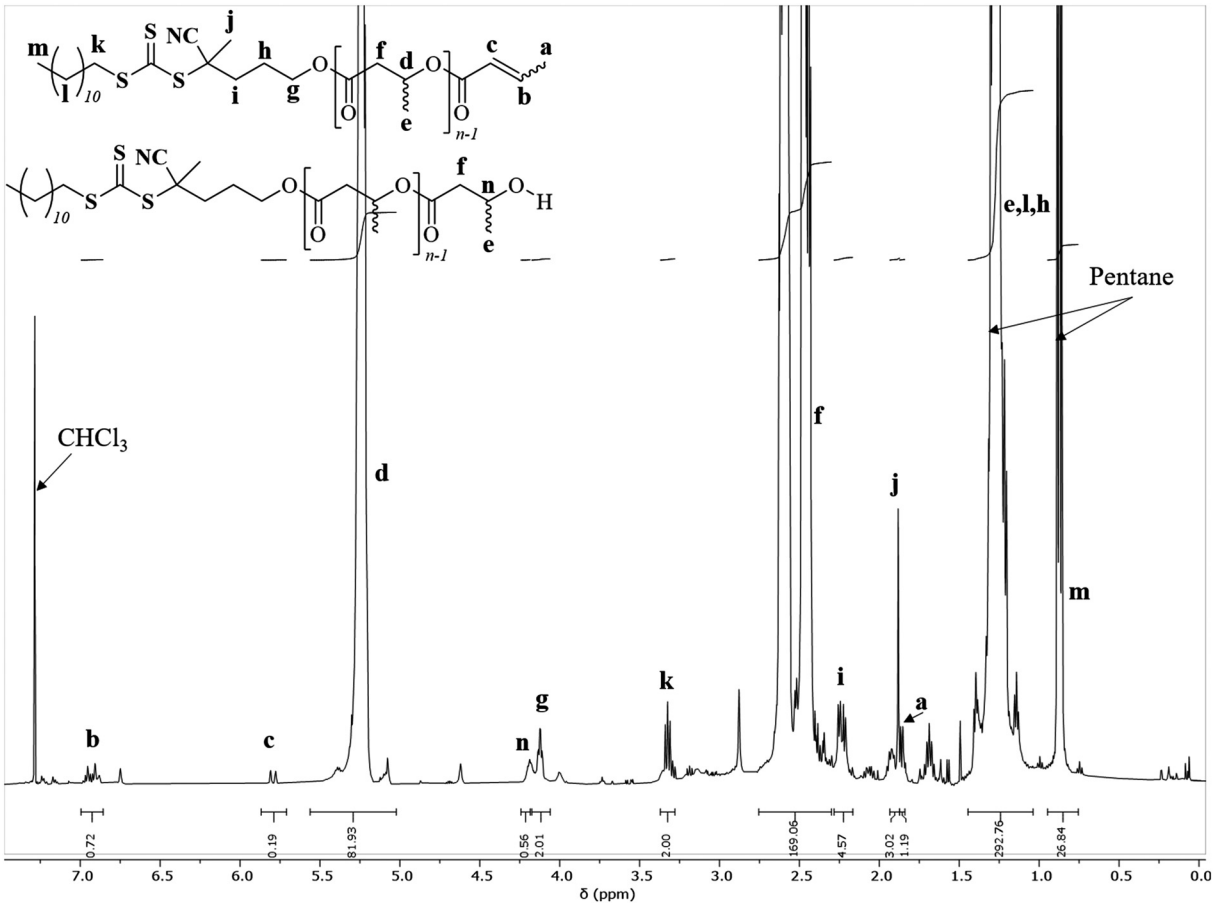

Fig. 1 ^{1}H NMR spectrum (500 MHz, $CDCl_3$, 25 °C) of PHB_{83}-TTC prepared by ROP of racemic β-butyrolactone catalyzed by Y{ONNO^{Me_2}} in the presence of TTC-OH (Table 1, entry 1).

crude mixture for the determination of the HEMA conversion (Fig. S3†), and by DLS, SEC in DMF, TEM and SAXS.

Results and discussion

The amphiphilic PHB-*b*-PHEMA diblock copolymers synthesized in THF comprise a solvophilic aliphatic polyester block, PHB, and a solvophobic methacrylic polymer block, PHEMA. Two different synthetic approaches were explored to first prepare the PHB-TTC macro-RAFT agent (Scheme 1).

Synthesis and characterization of the PHB-TTC precursor

A first strategy relying on the previously established organocatalyzed ROP of *rac*-β-BL mediated by the phosphazene base 2-*tert*-butylimino-2-diethylamino-1,3-dimethylperhydro-1,3,2-diazaphosphorine (BEMP), was first attempted. This was aimed at preparing an α-COOH, ω-crotonate telechelic PHB that would further be functionalized into a PHB-trithiocarbonate (TTC) by esterification with the TTC-OH chain transfer agent (Scheme 1a).[53] However, although the desired PHB-COOH polymer was initially formed, the following Steglich esterification in the presence of dicyclohexylcarbodiimide (DCC) and either dimethylaminopyridine (DMAP) or 2,6-lutidine, prompted the degradation of the resulting PHB-TTC, as monitored by ^{1}H NMR spectroscopy (Fig. S4†). We assumed that the DMAP or 2,6-lutidine base most likely altered the PHB stability. This contrasted with the previously reported successful esterification of the related poly(3-hydroxyoctanoate) using a similar Steglich esterification protocol.[17]

Alternatively, we implemented the well-known ROP of β-lactones mediated by yttrium-based catalytic systems in the presence of a hydroxyl end-capped TTC as initiating species.[1,9,16,49,50,54] The synthesis of the PHB first block was successfully achieved by ROP of *rac*-β-BL performed in toluene in the presence of a discrete yttrium catalyst supported by a tetradentate {ONNO^{Me_2}} dianionic ligand, and initiated by 4-cyano-4-[(dodecylsulfanylthiocarbonyl)sulfanyl]pentanol (TTC-OH) (Scheme 1b). This approach is similar to the recently reported ROP of L-lactide (LLA) catalyzed by DMAP in combination with an hydroxyl-terminated dithiocarbonate RAFT agent, affording a PLLA macroinitiator end-capped with the RAFT moiety, subsequently used for the copolymerization with various methacrylates.[55] The methyl-substituted Y{ONNO^{Me_2}} catalyst system was purposely selected so as to obtain *atactic* PHB segments that are typically more soluble than the more crystalline *iso*- or *syndio*-tactic ones. The work reported herein thus did not aim at varying the tacticity of the PHB precursor. PHB-TTC was synthesized with three different targeted degrees of polymerization (DP = 45, 70, 90), as tuned by the $[\beta\text{-BL}]_0/[\text{yttrium catalyst}]_0/[\text{TTC-OH}]_0$ molar ratio, with $[\text{TTC-OH}]_0 = [\text{yttrium catalyst}]_0$. The most relevant results are gathered in Table 1. High monomer conversions (85–96%) were reached, affording the expected telechelic PHB
α-end capped by the TTC RAFT agent moiety and ω-functionalized by either a crotonate or hydroxy group, as evidenced by ^{1}H and ^{13}C NMR (Fig. 1 and Fig. S2, S5, S6,† for PHB_n = PHB_{83}, PHB_{48}, and PHB_{57}, respectively, with *n* corresponding to the number of lactone repeating units), DOSY NMR (Fig. 2 and Fig. S7, and S8† for PHB_{83}, PHB_{48}, and PHB_{57}, respectively), as well as MALDI-ToF MS (Fig. 3, and Fig. S9† for PHB_{83} and PHB_{48}, respectively), and SEC (Fig. 4 and Fig. S10, and S11† for PHB_{83}, PHB_{48}, and PHB_{57}, respectively).

The PHB-TTC samples were characterized by detailed NMR spectroscopy. ^{1}H and ^{13}C NMR analyses revealed the formation of the expected α-TTC end-capped PHB, as evidenced by the TTC-RAFT agent signature (δ_{1H} = 3.32 ppm, CH_2–S–C═S, δ_{1H} = 4.12 ppm, CH_2–O–C═O; δ_{13C} = 217.4 ppm, S–*C*═S, δ_{13C} = 119.3 ppm, *C*N–C) (Fig. 1 and Fig. S3, S4, S5† for PHB_{83},

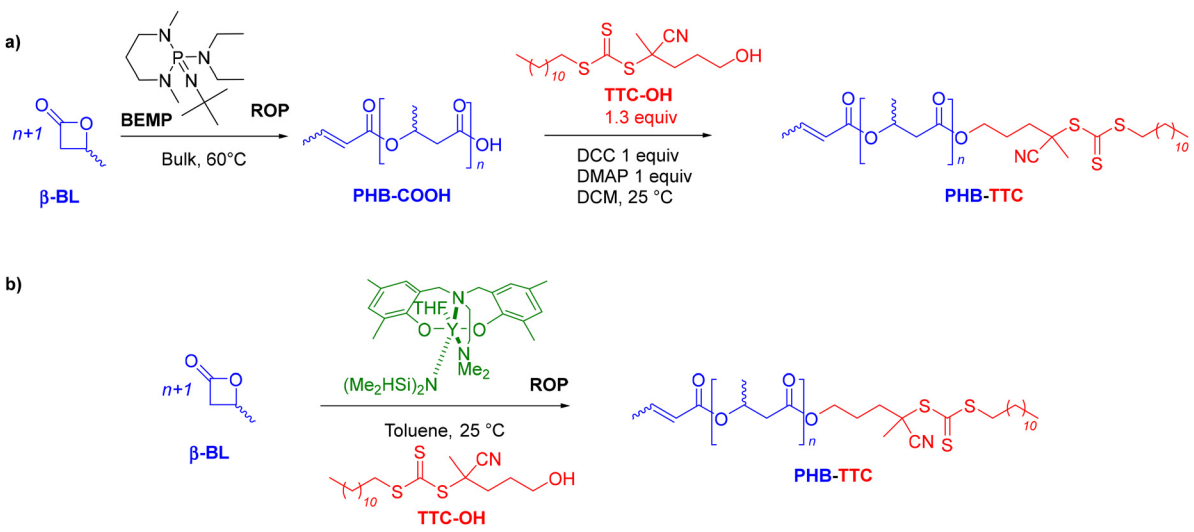

Scheme 1 Synthesis of PHB-TTC by ROP of *racemic* β-butyrolactone (*rac*-β-BL): (a) ROP promoted by an organic phosphazene base, BEMP, followed by esterification with TTC-OH, and, (b) ROP catalyzed by a discrete yttrium catalyst in the presence of TTC-OH as initiator.

Table 1 Macromolecular characteristics of PHB-TTC synthesized by ROP of racemic β-butyrolactone catalyzed by Y{ONNO^{Me_2}} (Y) in the presence of TTC-OH (Scheme 1b)

Entry	$[\beta\text{-BL}]_0/[Y]_0/[\text{TTC-OH}]_0$	Reaction time (h)	β-BL conv.[a] (%)	DP_{theo}[b]	$M_{n,theo}$[c] ($g.mol^{-1}$)	DP_{NMR}[d]	$M_{n,NMR}$[e] ($g.mol^{-1}$)	$M_{n,SEC}$[f] ($g.mol^{-1}$)	$Đ$[g]
1	90 : 1 : 1	3	92	83	7510	83	7500	9200	1.19
2	70 : 1 : 1	4	85	60	5510	57	5300	6600	1.24
3	45 : 1 : 1	3	96	43	4110	48	4500	6000	1.26

[a] Monomer conversion calculated by ^{1}H NMR analysis of the crude reaction mixture. [b] Theoretical degree of polymerization calculated using the β-BL conversion. [c] Molar mass calculated according to $M_{n,theo} = ([\beta\text{-BL}]_0/[\text{TTC-OH}]_0 \times \text{conv.}_{\beta\text{-BL}} \times M_{\beta\text{-BL}}) + M_{TTC-OH}$ with $M_{\beta\text{-BL}} = 86$ g mol^{-1} and $M_{TTC-OH} = 390$ g mol^{-1}. [d] Experimental degree of polymerization determined by ^{1}H NMR end-group analysis. [e] Molar mass determined by ^{1}H NMR analysis of the isolated polymer, from the resonances of the terminal TTC group. [f] Number-average molar mass determined by SEC in THF *vs.* polystyrene standards. [g] Dispersity ($Đ = M_w/M_n$) determined by SEC analysis in THF.

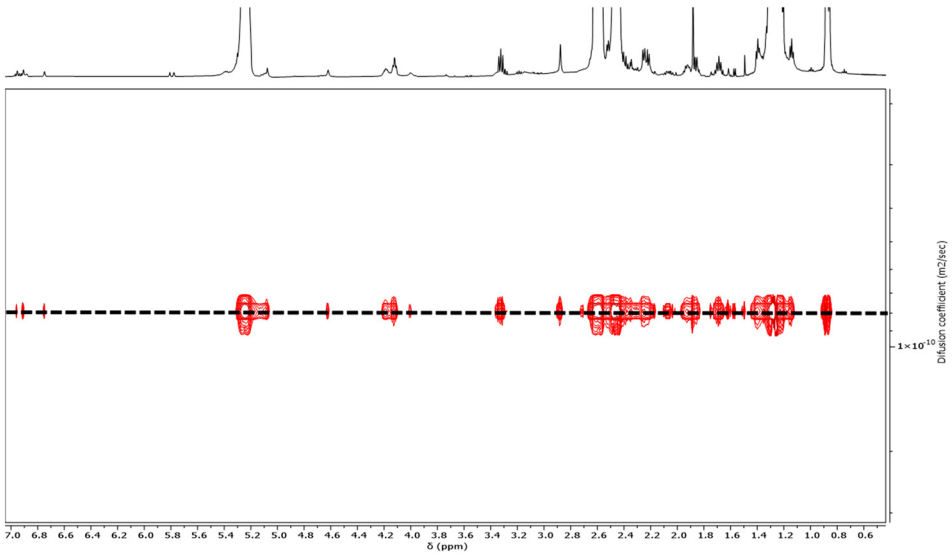

Fig. 2 DOSY NMR spectrum (500 MHz, $CDCl_3$, 25 °C) of PHB_{83}-TTC prepared by ROP of racemic β-butyrolactone catalyzed by Y{ONNO^{Me_2}} and initiated by TTC-OH (Table 1, entry 1).

PHB_{48}, and PHB_{57}, respectively). Evidence of a population of PHB hydroxy-terminated was observed (δ_{1H} = 4.14 ppm, C*H*(CH_3)–OH; δ_{13C} = 43.7 ppm, *C*H(CH_3)–OH). The formation of some ω-crotonate PHB (δ_{1H} = 6.95 ppm, CH_3–C*H*═CH, δ_{1H} = 5.81 ppm, *C*H_3–CH═C*H*; δ_{13C} = 124.8 ppm, CH_3–*C*H═CH, δ_{13C} = 122.7 ppm, *C*H_3–CH═*C*H) resulted from the elimination of H_2O from the above-mentioned hydroxy-end capped PHB chains, as classically observed in the ROP of β-BL.[53] The DP values calculated by ^{1}H NMR analysis, based on the *C*H_2–S–C═S methylene signal of the TTC end-group (present on all chains), were found in good agreement with the targeted values (Table 1). Moreover, the DOSY NMR spectrum displayed a single diffusion coefficient, further corroborating the purity of the PHB-TTC functional polymer thus prepared by ROP (Fig. 2).

MALDI-ToF mass spectrometry investigations enabled to gain deeper insights into the macromolecular structure and topology of the PHB-TTC. The MALDI-ToF mass spectrum, recorded using a DCTB matrix, of PHB_{83}-TTC typically showed a main population corresponding to PHB end-capped by both the TTC and the crotonate moieties, as anticipated from the ROP of *rac*-β-butyrolactone catalyzed by Y{ONNO^{Me_2}} and initiated by TTC-OH (Fig. 3a and Fig. S9† for PHB_{83} and PHB_{48}, respectively). Another population corresponding to the HO-PHB_n-TTC with a hydroxyl end-group was also observed. These findings were supported by the good match between the corresponding experimental and simulated populations, respectively (Fig. 3c and d). The other minor populations of PHB chains could not be unambiguously assigned.

The PHB-TTC samples were fully soluble in THF at room temperature, thereby enabling their SEC analysis in this eluent (Fig. 4). The experimental molar mass values determined by NMR ($M_{n,NMR}$) matched quite well with the theoretical data ($M_{n,theo}$), while SEC values ($M_{n,SEC}$, not corrected) were found slightly higher, most likely due to the different hydrodynamic radius of the polystyrene standards used for calibration. The dispersities $Đ = M_w/M_n$ remained lower than 1.26, indicating a good control of the ROP. Furthermore, SEC measurements of a PHB-TTC using a photo-diode array detector operating at wavelengths from 200 to 400 nm, returned an isoabsorbance plot

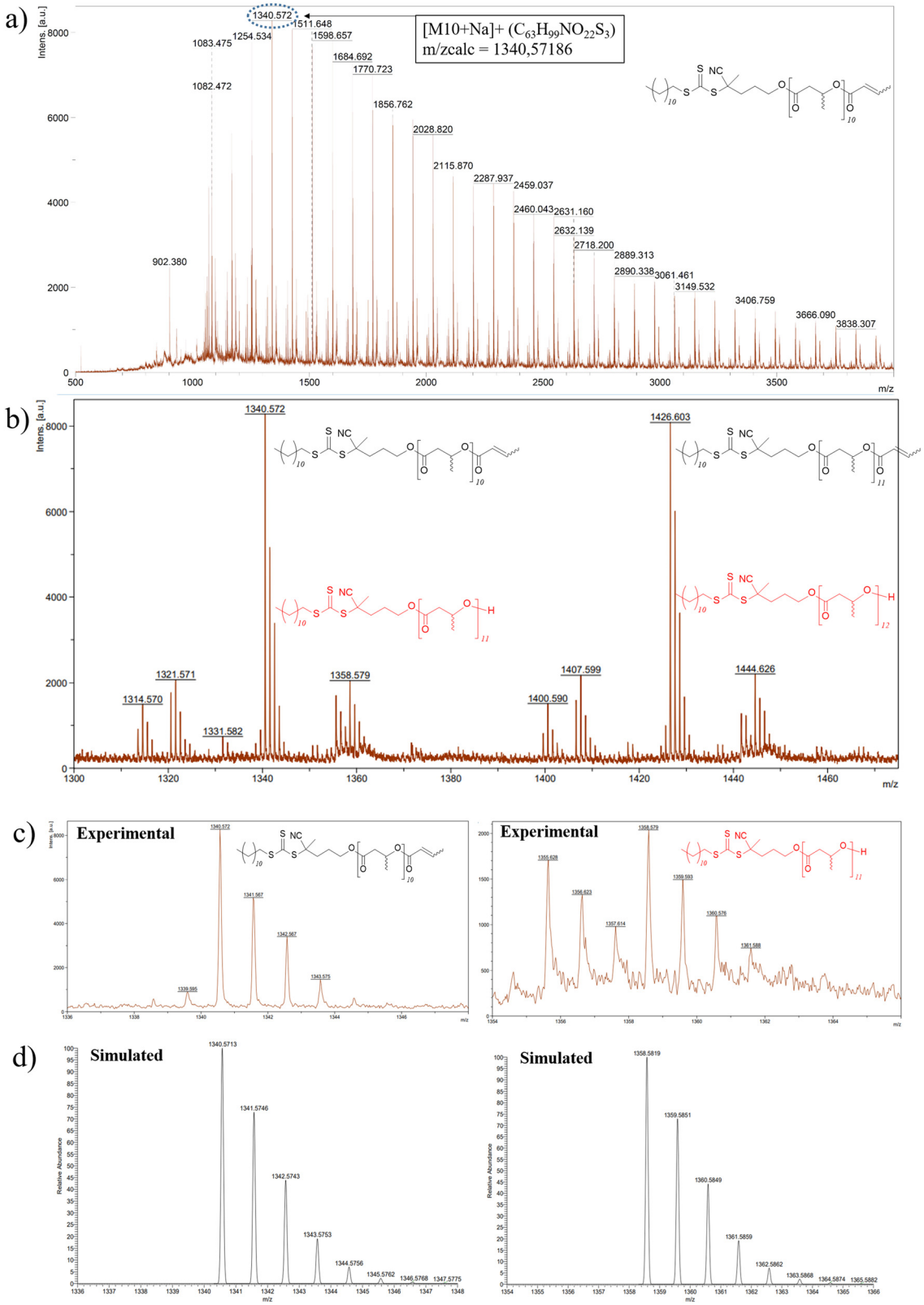

Fig. 3 (a) High resolution MALDI-ToF mass spectrum (DCTB matrix, ionized by Na^+), of PHB_{83}-TTC prepared by ROP of *racemic* β-butyrolactone catalyzed by Y{ONNO^{Me}} and initiated by TTC-OH (Table 1, entry 1). The lower molar mass macromolecules are observed with *m*/*z* experimental (m/z_{exp}) *vs.* calculated (m/z_{calc}) values, respectively, for the crotonate-PHB_{83}-TTC for: DP = 9: 1254.534 *vs.* 1254.535; DP = 10: 1340.572 *vs.* 1340.572; DP = 11: 1426.603 *vs.* 1426.609; DP = 20: 2200.909 *vs.* 2200.939, (b) zoom and assignment of the two major populations crotonate-PHB_{83}-TTC and HO-PHB_{83}-TTC, (c) zoom of the major population crotonate-PHB_{83}-TTC (DP = 10 and DP = 11) and the minor population HO-PHB_{83}-TTC (DP = 11 and DP = 12), (d) simulation of the above major and minor populations, respectively.

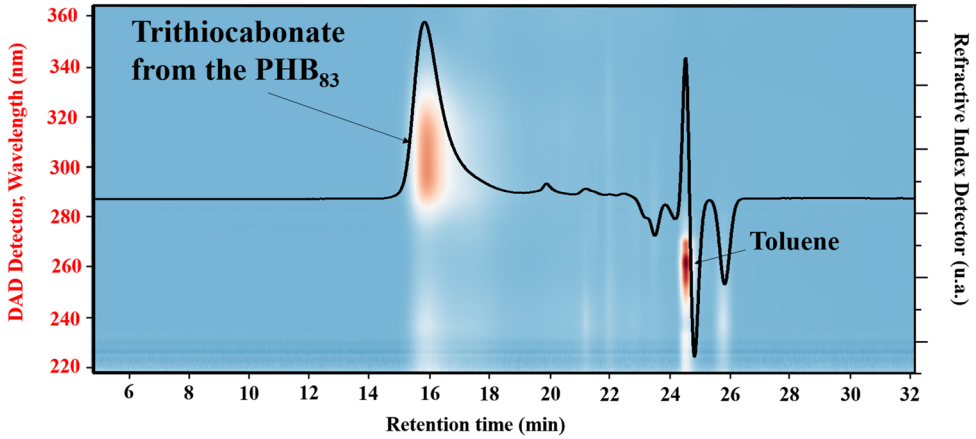

Fig. 4 SEC chromatogram in THF superimposed with the isoabsorbance plot of PHB_{83}-TTC prepared by ROP of *racemic* β-butyrolactone catalyzed by Y{ONNO^{Me_2}} in the presence of TTC-OH (Table 1 entry 1).

displaying an intense elution spot at 310 nm, which corresponds to the TTC moiety of the PHB-TTC (Fig. 4 and Fig. S10, S11† for PHB_{83}, PHB_{48}, and PHB_{57}, respectively).[56] Rewardingly, the refractive index signal clearly matched with the UV signal, thus supporting the PHB end-capping by the TTC moiety.

Synthesis and characterization of the PHB-*b*-PHEMA block copolymers

Chain extension of the PHB_{83}-TTC acting as the macro-RAFT agent with HEMA was performed in THF, a good solvent of the RAFT-macroinitiator, at 60 °C in the presence of AIBN (typical PISA operating conditions: $[AIBN]_0/[PHB\text{-}TTC]_0$ = 1 : 5; Scheme 2 and Table 2). HEMA was selected as the methacrylate monomer as it satisfies the PISA requirements, namely the solubility as a monomer in the copolymerization solvent, and the insolubility of the corresponding (co)polymer segment in that same solvent.[57] Thus, at the early stage of the copolymerization, all components were soluble and, as the PISA proceeded, the reaction mixture became cloudier-to-turbid, clearly visually showing a dispersion of the copolymer in THF (Fig. S12†).

Four series of PHB_{83}-*b*-$PHEMA_y$ were synthesized in THF at 60 °C, by varying the length of the polymethacrylate block with 200, 350, or 500 *y* repeating units, at different initial PHB-TTC macro-RAFT agent and HEMA concentrations, the latter ranging from 5 to 15wt% (Table 2). The HEMA comonomer conversion, as determined by ^{1}H NMR in DMSO-d_6 of the final mixture recovered after 20 h, revealed greater than 77% in all cases. At the lowest comonomer and PHB-TTC macro-RAFT agent composition of 5wt%, the HEMA conversion ranged from 77 to 80% which is the lowest conversion detected for the whole range of composition investigated, as anticipated. On the other hand, at the higher compositions of 7.5, 10 or 15wt%, the HEMA conversion significantly increased (86–95%), returning copolymers with a longer polymethacrylate segment.

The corresponding SEC chromatograms of the PHB-*b*-PHEMA samples analyzed in DMF clearly showed the shift of the trace of the PHB_{83}-TTC to lower elution volumes, proportionally to the increase of the DP_{HEMA} ranging from 200 to 500 units, respectively. This demonstrated the successful chain extension from the macro-RAFT agent upon copolymerizing with HEMA (Table 2 and Fig. 5). All the chromatograms were not ideally monomodal, showing small low and high molar mass shoulders, especially the one (green trace) corresponding to DP_{HEMA} of 500 at 15wt% (Table 2, entry 12; Fig. 5). Accordingly, the dispersity values were slightly enlarged. This suggested a non-fully optimized control of the RAFT polymerization, possibly due to a slower initiation as compared to the propagation and/or to some undesirable side reactions (typically termination reactions). This may arise from the fact that

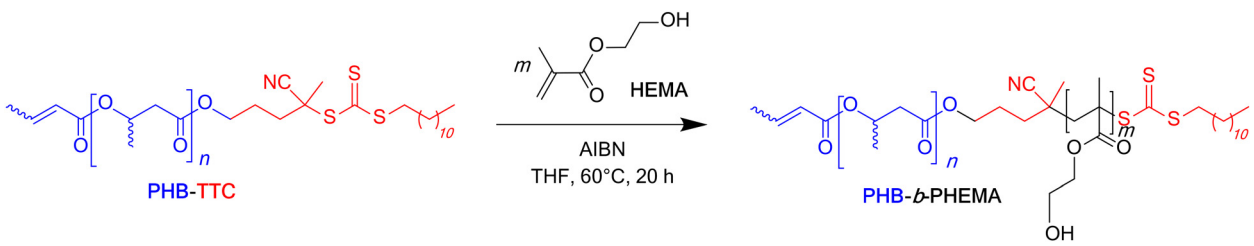

Scheme 2 Synthesis of PHB-*b*-PHEMA diblock copolymers by RAFT dispersion polymerization of HEMA from PHB-TTC macro-RAFT agents.

Table 2 Characteristics of PHB-*b*-PHEMA diblock copolymers and resulting nano-objects prepared from PHB_{83}-TTC macro-RAFT agent and HEMA RAFT/PISA polymerization

Entry	[HEMA + PHB-TTC] [a] (wt%)	DP_{HEMA} targeted [b]	$Conv_{HEMA}$ [c] (%)	DP_{HEMA} [d] Calc	$M_{n,SEC}$ [e] ($g.mol^{-1}$)	$Đ$ [f]	$D_{H,DLS}$ [g] (nm)	PDI_{DLS} [h]	$D_{app,TEM}$ [i] (nm)	SD_{TEM} [j] (nm)
0	PHB_{83}	—		—	8300	1.20	—	—	—	—
1	5	200	78	157	38 480	1.75	56	0.09	208	106
2	5	350	80	281	72 200	1.71	83	0.07	179	90
3	5	500	77	387	104 300	1.81	164	0.03	316	128
4	7.5	200	94	189	39 530	1.77	62	0.04	171	59
5	7.5	350	95	331	64 580	1.79	85	0.10	252	90
6	7.5	500	86	431	84 240	1.88	176	0.11	163	44
7	10	200	84	168	66 000	1.66	72	0.06	N/A [k]	N/A [k]
8	10	350	91	319	86 160	1.83	83	0.07	N/A [k]	N/A [k]
9	10	500	90	450	108 400	1.72	178	0.03	134	30
10	15	200	84	168	53 040	1.60	85	0.14	151	84
11	15	350	91	319	84 150	1.82	123	0.12	197	57
12	15	500	91	455	109 500	2.55	194	0.02	255	78

[a] Initial HEMA monomer weight added to PHB-TTC macro-RAFT agent weight *vs.* THF weight in wt%. [b] Targeted degree of polymerization of HEMA. [c] HEMA monomer conversion as calculated by ^{1}H NMR analysis. [d] Calculated degree of polymerization of PHEMA as established from $DP_{HEMA,targeted} \times X_{HEMA}$. [e] Number-average molar mass as determined by SEC in DMF *vs.* polystyrene standards. [f] Dispersity as determined by SEC in DMF. [g] Hydrodynamic diameter of the particles formed from PHB-*b*-PHEMA, as measured by DLS. [h] Polydispersity index of the particles formed from PHB-*b*-PHEMA as measured by DLS. [i] Apparent diameter of the particles formed from PHB-*b*-PHEMA as measured from TEM. [j] Standard deviation of the apparent diameter of the particles formed from PHB-*b*-PHEMA as measured from two TEM micrographs by Image J (Fig. S13–S22†). [k] Micrograph not taken by TEM.

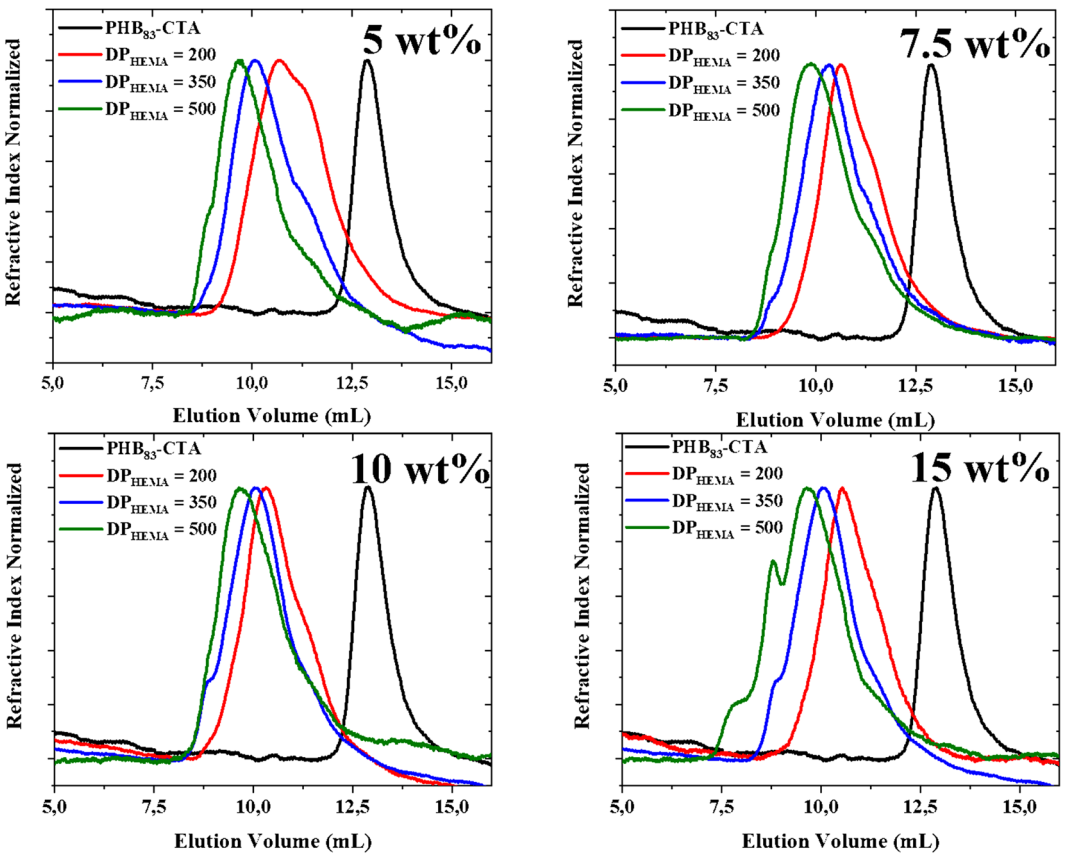

Fig. 5 SEC chromatograms (DMF, 25 °C) of PHB_{83}-TTC macro-RAFT agent (black trace) and of the dispersions made at four different initial concentrations of HEMA *i.e.* 5 wt%, 7.5 wt%, 10 wt% and 15 wt% for different targeted degrees of polymerization, DP = 200 (red trace), 350 (blue trace) and 500 (green trace).

the block copolymerization were performed in THF, a solvent from which residual traces of peroxides may to some extent be deleterious to the TTC group.[58] The latter above-mentioned shoulder at high molar mass suggested a branched architecture, which most likely arose from residual ethylene glycol dimethacrylate impurity within HEMA.[59,60] This monomer contaminant most probably acted as a branching agent and accounted for the high dispersity values observed for the corresponding diblock copolymers ($1.60 < Đ < 1.88$), except for the composition targeting 500 HEMA units at 15 wt% ($Đ = 2.55$) (Table 2, entry 12). Besides, the presence of a low molar mass shoulder in the SEC traces could arise from the presence of a few PHB segments void of the RAFT terminal/initiating group in the prepolymer; however, these could not be unambiguously identified in the MALDI-ToF mass spectrum. In any case, the shift of the retention time between the black trace of the TTC end-capped PHB prepolymer and the three other colored traces of the PHB_x-*b*-$PHEMA_y$ copolymers clearly suggested that a block copolymerization occurred as mediated by RAFT, thereby supporting that the polymerization was controlled to some extent.

The dispersions of PHB_{83}-*b*-$PHEMA_y$ diblock copolymers in THF were further analyzed using dynamic light scattering (DLS) (Table 2). Narrow monomodal distributions of the scattered intensity as a function of hydrodynamic diameters with PDI < 0.14 were recorded for all dispersions. These are gathered in a pseudo-phase diagram showing the evolution of the hydrodynamic diameter with the initial weight percentage of comonomer and PHB-TTC *vs.* THF as the *x*-axis and to the targeted DP of HEMA as the *y*-axis (Fig. 6). The hydrodynamic diameter D_H of the particles was found to increase monotonously, according to the targeted DP_{HEMA} and also to the initial weight percentage of comonomer and PHB-TTC along the pseudo-phase diagram, as expected. The D_H values varied from 56 to 194 nm along with a relatively low polydispersity index ($0.02 <$ PDI < 0.14) (Table 2, entries 1–12).[61] This indicated that the size of PHB_{83}-*b*-$PHEMA_y$ particles were narrowly dispersed in THF.

The morphology of the particles generated within the dispersions were investigated by transmission electron microscopy (TEM) analyses. TEM analysis of such type of PHA-based copolymer dispersions revealed difficult due to the unusual solvent used, *i.e.* THF. Typical micrographs are illustrated in the ESI (Fig. S13–S22†). As a general trend, the apparent hydrodynamic diameter D_{app} (apparent diameter ranging from 134 to 316 nm) determined by Image J on two different micrographs, taking at least 50 particles, returned values higher than D_{DLS} ones (56 to 194 nm) (Table 2). Larger and more polydisperse particles were observed by TEM as compared to the corresponding DLS measurements, most likely arising from the sample preparation and from the different physical states between the solution analyzed by DLS and the dried sample captured by TEM. Hence, this difference may result from the adsorption of these particles onto the surface, which may cause a slight spreading and, consequently, an increase in their lateral dimension, as previously observed in

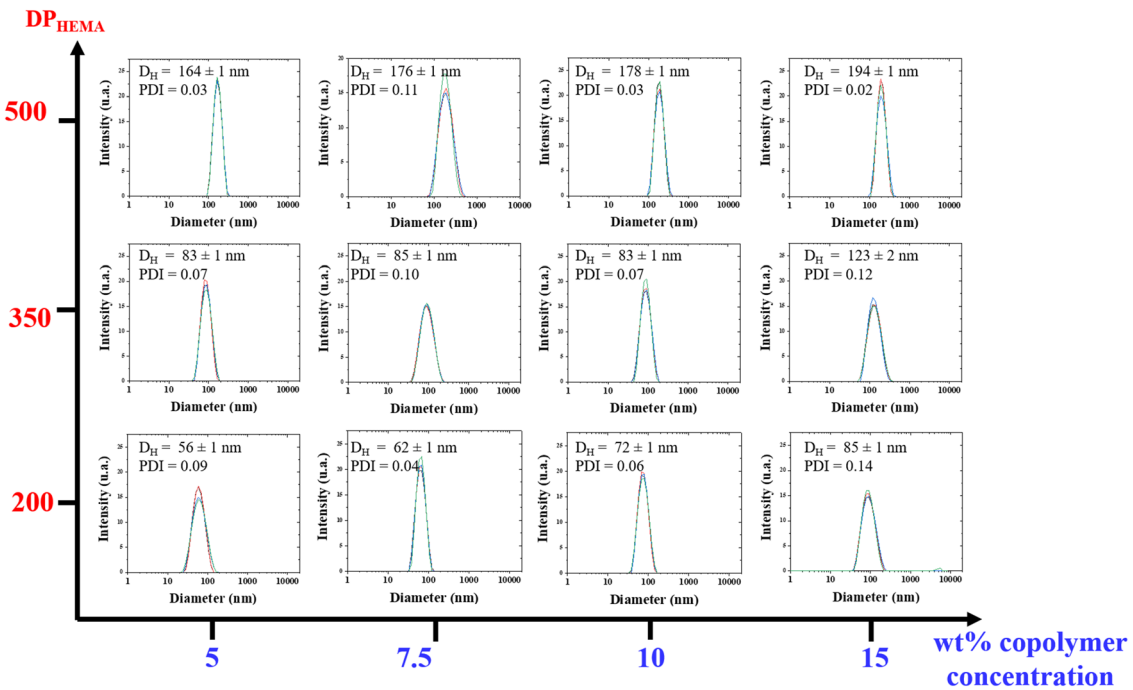

Fig. 6 Intensity-averaged size distribution obtained by DLS for each PHB_{83}-*b*-$PHEMA_y$ dispersion, showing the evolution of the hydrodynamic diameters (D_H in nm) and PDI, with the increase of the DP_{HEMA} and with the initial weight concentration of the PHB_{83}-TTC macro-RAFT agent added to the monomer weight *vs.* THF (wt% copolymer concentration) for the PHB_{83}-TTC macro-RAFT agent. DLS measurements were performed in triplicate for each sample.

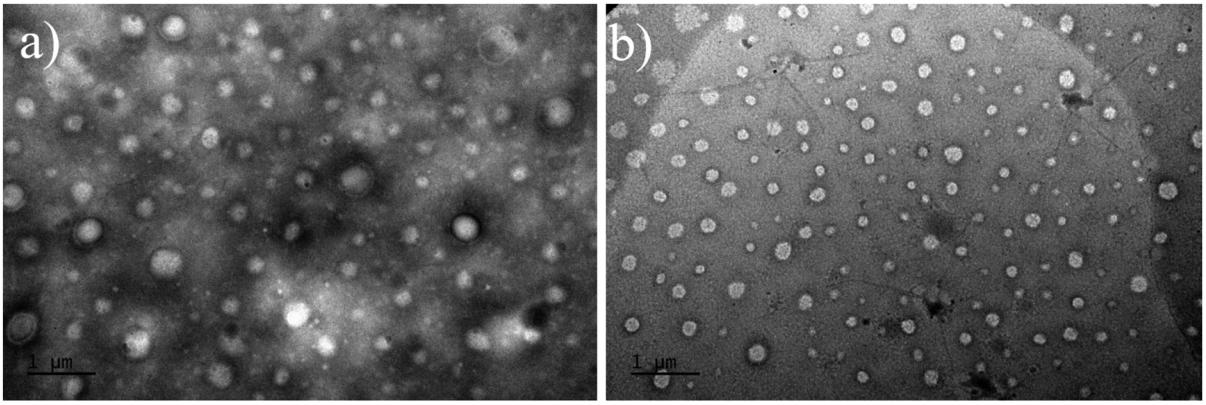

Fig. 7 TEM micrographs of PHB_{83}-*b*-$PHEMA_{500}$ made at (a) 5 wt% and (b) 7.5 wt% of HEMA comonomer and PHB_{83}-TTC macro-RAFT agent concentration.

other polymer systems.[62] Furthermore, some spheres exhibited a vesicular shape, with thin membranes being clearly distinguished (Fig. 7a and Fig. S13, S14, S15, S20†), suggesting the coexistence of vesicles and micelles in the dried samples prepared for TEM. These results further demonstrated that a PISA process was indeed proceeding smoothly during the copolymerization of HEMA from the PHB_{83}-TTC macro-RAFT agent in THF. As stated in the literature, PISA offers a highly effective approach for designing and producing a diverse array of block copolymer nano-objects, including spheres, worms, and vesicles, in different media.[18–41]

SAXS experiments were performed on two samples in order to better understand the morphology of the particles. Fig. 8 shows the SAXS patterns of PHB_{83}-*b*-$PHEMA_{500}$ at 5 and 7.5 wt% of HEMA comonomer and macro-RAFT agent concentration. The gradient in the low q region of both patterns is about −2.5, exhibiting the presence of vesicles in the suspension, as already stated in the literature.[63] This result is in agreement with the TEM images showing spherical particles with morphologies most-likely corresponding to those of vesicles (Fig. 7). After fitting the data by using a spherical vesicle model, the two local minima of both patterns were investigated.[64] The minima observed at 1.3–1.4 × 10^{-2} $Å^{-1}$ gives information about the vesicle membrane thickness, and the one around 3 × 10^{-3} $Å^{-1}$ highlights the overall vesicle size. It was found that for both compositions, the membrane thickness is about 50 nm, and the overall vesicle diameter around 195–200 nm. These particle sizes are in the same range as the hydrodynamic diameters obtained by DLS (Fig. 6).

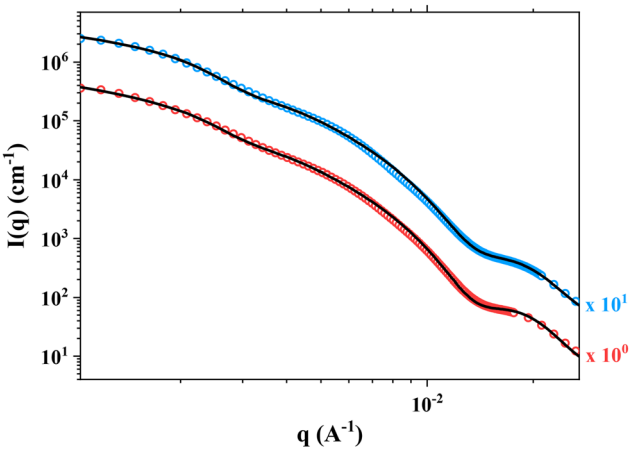

Fig. 8 SAXS patterns of PHB_{83}-*b*-$PHEMA_{500}$ prepared at 5 wt% (in red) and 7.5 wt% (in blue) of HEMA comonomer and PHB_{83}-TTC macro-RAFT agent concentration. The data fits obtained by using a spherical vesicle model is shown in black solid lines. The *I*(*q*) profiles were multiplied by a constant indicated on the Figure, so as to improve its readability.

Conclusion

PHB-TTC macro-RAFT agent samples were successfully synthesized by ROP of *rac*-β-BL catalyzed by an *in situ* generated yttrium alkoxide complex in the presence of a TTC-OH initiator. Well-defined α-crotonate (and also α-OH),ω-TTC PHBs ($M_{n,NMR}$ up to 7500 g mol^{-1}, $Đ$ *ca.* 1.19) recovered polyesters, as characterized by NMR spectroscopy, MALDI-ToF mass spectrometry and SEC analyses, supported a controlled polymerization. Their subsequent use as macro-RAFT agent in the synthesis of dispersion copolymers *via* RAFT PISA copolymerization of HEMA in THF, represents the first use of a PHA in a PISA process, to elaborate, in the present study, PHA/polymethacrylate nanoparticles. The resulting PHB-*b*-PHEMA copolymers were obtained with a noticeable increase of the molar mass from the PHB-TTC precursor. Particle sizes were found to increase with larger initial concentration of comonomer added to the macro-RAFT agent. The same effect was similarly observed with the increase of the length of the second PHEMA block. TEM observations confirmed the existence of particles formed through the PISA process, presenting a spherical shape corresponding to micelles, presumably, and in some cases, a vesicular shape. SAXS measurements performed on PHB_{83}-*b*-

$PHEMA_{500}$ at 5 wt% and 7.5 wt% of HEMA comonomer and macro-RAFT agent revealed the presence of vesicles in the suspension, in good agreement with TEM observations. This ROP/RAFT/PISA process thus paves the way to our on-going investigations on dispersions formed in water upon copolymerizing from a hydrophilic PHA precursor, ultimately leading to pharmaceutical applications.

Author contributions

Julien Rosselgong: investigation, formal analysis, conceptualization, writing – original draft, review and editing. Ali Dhaini: investigation, formal analysis. Manon Rochedy: SAXS analysis, data curation, writing – original draft. Lourdes Mónica Bravo-Anaya: SAXS, TEM and DLS analyses, writing – original draft, review and editing. Jean-François Carpentier: writing – original draft, review and editing, funding acquisition, formal analysis. Sophie M Guillaume: writing – original draft, review and editing, supervision, formal analysis, funding acquisition and conceptualization.

Data availability

The raw data required to reproduce these findings are available from the authors. The processed data required to reproduce these findings are available in the ESI.†

Conflicts of interest

The authors declare no conflicts of interest.

Acknowledgements

Jérôme Ollivier (ISCR) and Philippe Jehan (ScanMAT, UAR2025, University of Rennes) are thanked for MALDI-ToF MS analyses and fruitful discussions. Agnès Burel (UMS Biosit University of Rennes) is acknowledged for useful discussions regarding TEM images, and Ludivine Rault for TEM analyses (ScanMAT, UAR2025, University of Rennes). Ma. Lizbeth Zepeda García is acknowledged for her help in TEM images analysis. Javier Perez (Synchrotron SOLEIL, F-91192, Gif-sur-Yvette) and the BAG 20231446 (SLAMM) are warmly thanked for the opportunity to perform SAXS experiments on the SWING beamline of SOLEIL facilities. The authors acknowledge financial support from GDR2019 CNRS/INRAE "Solliciter LA Matière Molle" (SLAMM) and from the Synchrotron Soleil (beamline SWING). Prof. Steve Armes (University of Sheffield, UK) and Dr Matthew Derry (Aston University, UK) are gratefully acknowledged for fruitful discussions.

References

1 G. Barouti, C. G. Jaffredo and S. M. Guillaume, Advances in drug delivery systems based on synthetic poly(hydroxybutyrate) (co)polymers, *Prog. Polym. Sci.*, 2017, **73**, 1–31.
2 J. Mai, K. Kockler, E. Parisi, C. M. Chan, S. Pratt and B. Laycock, Synthesis and physical properties of polyhydroxyalkanoate (PHA)-based block copolymers: a review, *Int. J. Biol. Macromol.*, 2024, **263**, 130204.
3 Z. Luo, Y.-L. Wu, Z. Li and X. J. Loh, Recent progress in polyhydroxyalkanoates-based copolymers for biomedical applications, *Biotechnol. J.*, 2019, **14**, 1900283.
4 M. Koller, *The handbook of polyhydroxyalkanoates,* CRC Press, 1st edn, 2020, vol. 1–3.
5 S. Taguchi, T. Iwata, H. Abe and Y. Doi, in *Polymer Science: A Comprehensive Reference*, ed. K. Matyjaszewski, and M. Mçller, Elsevier, London, 2012, Vol. 9, pp. 157–182.
6 A. H. Westlie, E. C. Quinn, C. R. Parker and E. Y.-X. Chen, Synthetic biodegradable polyhydroxyalkanoates (PHAs): Recent advances and future challenges, *Prog. Polym. Sci.*, 2022, **134**, 101608.
7 J. K. Muiruri, J. C. C. Yeo, Q. Zhu, E. Ye, X. J. Loh and Z. Li, Poly(hydroxyalkanoates): production, applications and end-of-life strategies–life cycle assessment nexus, *ACS Sustainable Chem. Eng.*, 2022, **10**, 3387–3406.
8 A. Dhaini, V. Hardouin-Duparc, A. Alaaeddine, J.-F. Carpentier and S. M. Guillaume, Recent advances in polyhydroxyalkanoates degradation and chemical recycling, *Prog. Polym. Sci.*, 2024, **149**, 101781.
9 G. Barouti, S. S. Liow, Q. Dou, H. Ye, C. Orione, S. M. Guillaume and X. J. Loh, New linear and star–shaped thermogelling poly([R]–3−hydroxybutyrate) copolymers, *Chem. – Eur. J.*, 2016, **22**, 10501–10512.
10 X. J. Loh, Z.-X. Zhang, Y.-L. Wu, T. S. Lee and J. Li, Synthesis of novel biodegradable Thermoresponsive triblock copolymers based on poly[(R)-3-hydroxybutyrate] and poly(N-isopropylacrylamide) and their formation of thermoresponsive micelles, *Macromolecules*, 2009, **42**, 194–202.
11 X. J. Loh, W. C. D. Cheong, J. Li and Y. Ito, Novel poly(N-isopropylacrylamide)-poly[(R)-3-hydroxybutyrate]-poly(N-isopropylacrylamide) triblock copolymer surface as a culture substrate for human mesenchymal stem cells, *Soft Matter*, 2009, **5**, 2937–2946.
12 N. Corrigan, K. Jung, G. Moad, C. J. Hawker, K. Matyjaszewski and C. Boyer, Reversible-deactivation radical polymerization (Controlled/living radical polymerization): From discovery to materials design and applications, *Prog. Polym. Sci.*, 2020, **111**, 101311.
13 M. K. Georges, R. P. N. Veregin, P. M. Kazmaier and G. K. Hamer, Narrow molecular weight resins by a free-radical polymerization process, *Macromolecules*, 1993, **26**, 2987–2988.
14 J.-S. Wang and K. Matyjaszewski, Controlled/" living" radical polymerization. Halogen atom transfer radical polymerization promoted by a Cu(I)/Cu(II) redox process, *Macromolecules*, 1995, **28**, 7901–7910.

15 J. Chiefari, Y. K. Chong, F. Ercole, J. Krstina, J. Jeffery, T. P. T. Le, R. T. A. Mayadunne, G. F. Meijs, C. L. Moad, G. Moad, E. Rizzardo and S. H. Thang, Living free-radical polymerization by reversible addition-fragmentation chain transfer: the RAFT process, *Macromolecules*, 1998, **31**, 5559–5562.

16 G. Barouti, S. S. Liow, Q. Dou, H. Ye, C. Orione, S. M. Guillaume and X. J. Loh, New linear and star–shaped thermogelling poly([R]–3–hydroxybutyrate) copolymers, *Chem. – Eur. J.*, 2016, **22**, 10501–10512.

17 B. Hazer, M. Eren, Y. Senemoğlu, E. Renard and V. Langlois, Novel poly(3-hydroxy butyrate) macro RAFT agent. Synthesis and characterization of thermoresponsive block copolymers, *J. Polym. Res.*, 2020, **27**, 1–12.

18 N. J. Penfold, J. Yeow, C. Boyer and S. P. Armes, Emerging trends in polymerization-induced self-assembly, *ACS Macro Lett.*, 2019, **8**, 1029–1054.

19 N. J. Warren and S. P. Armes, Polymerization-induced self-assembly of block copolymer nano-objects via RAFT aqueous dispersion polymerization, *J. Am. Chem. Soc.*, 2014, **136**, 10174–10185.

20 S. L. Canning, G. N. Smith and S. P. Armes, A critical appraisal of RAFT-mediated polymerization-induced self-assembly, *Macromolecules*, 2016, **49**, 1985–2001.

21 M. J. Derry, L. A. Fielding and S. P. Armes, Polymerization-induced self-assembly of block copolymer nanoparticles via RAFT non-aqueous dispersion polymerization, *Prog. Polym. Sci.*, 2016, **52**, 1–18.

22 J. Rieger, Guidelines for the synthesis of block copolymer particles of various morphologies by RAFT dispersion polymerization, *Macromol. Rapid Commun.*, 2015, **36**, 1458–1471.

23 B. Charleux, G. Delaittre, J. Rieger and F. D'Agosto, Polymerization-induced self-assembly: from soluble macromolecules to block copolymer nano-objects in one step, *Macromolecules*, 2012, **45**, 6753–6765.

24 A. Blanazs, J. Madsen, G. Battaglia, A. J. Ryan and S. P. Armes, Mechanistic insights for block copolymer morphologies: how do worms form vesicles?, *J. Am. Chem. Soc.*, 2011, **133**, 16581–16587.

25 A. Blanazs, R. Verber, O. O. Mykhaylyk, A. J. Ryan, J. Z. Heath, C. W. Douglas and S. P. Armes, Sterilizable gels from thermoresponsive block copolymer worms, *J. Am. Chem. Soc.*, 2012, **134**, 9741–9748.

26 S. J. Byard, M. Williams, B. E. McKenzie, A. Blanazs and S. P. Armes, Preparation and cross-linking of all-acrylamide diblock copolymer nano-objects via polymerization-induced self-assembly in aqueous solution, *Macromolecules*, 2017, **50**, 1482–1493.

27 Y. Jiang, N. Xu, J. Han, Q. Yu, L. Guo, P. Gao, X. Lu and Y. Cai, The direct synthesis of interface-decorated reactive block copolymer nanoparticles via polymerisation-induced self-assembly, *Polym. Chem.*, 2015, **6**, 4955–4965.

28 W. Shen, Y. Chang, G. Liu, H. Wang, A. Cao and Z. An, Biocompatible, antifouling, and thermosensitive core-shell nanogels synthesized by RAFT aqueous dispersion polymerization, *Macromolecules*, 2011, **44**, 2524–2530.

29 C. Grazon, J. N. Rieger, N. Sanson and B. Charleux, Study of poly(N,N-diethylacrylamide) nanogel formation by aqueous dispersion polymerization of N,N-diethylacrylamide in the presence of poly(ethylene oxide)-b-poly(N,N-dimethylacrylamide) amphiphilic macromolecular RAFT agents, *Soft Matter*, 2011, **7**, 3482–3490.

30 D. Ikkene, J.-L. Six and K. Ferji, Progress in aqueous dispersion RAFT PISA, *Eur. Polym. J.*, 2023, **188**, 111848–111867.

31 S. W. Thompson, T. R. Guimarães and P. B. Zetterlund, Multiblock copolymer synthesis via aqueous RAFT polymerization-induced self-assembly (PISA), *Polym. Chem.*, 2022, **13**, 5048–5057.

32 M. Semsarilar, N. J. W. Penfold, E. R. Jones and S. P. Armes, Semi-crystalline diblock copolymer nano-objects prepared via RAFT alcoholic dispersion polymerization of stearyl methacrylate, *Polym. Chem.*, 2015, **6**, 1751–1757.

33 Y. Pei, N. C. Dharsana and A. B. Lowe, Ethanolic RAFT dispersion polymerization of 2-(Naphthalen-2-yloxy)ethyl methacrylate and 2-phenoxyethyl methacrylate with poly[2-(dimethylamino)ethyl methacrylate] macro-chain transfer agents, *Aust. J. Chem.*, 2015, **68**, 939–945.

34 Y. Pei, N. C. Dharsana, J. A. van Hensbergen, R. P. Burford, P. J. Roth and A. B. Lowe, RAFT dispersion polymerization of 3-phenylpropyl methacrylate with poly[2-(dimethylamino)ethyl methacrylate] macro-CTAs in ethanol and associated thermoreversible polymorphism, *Soft Matter*, 2014, **10**, 5787–5796.

35 E. R. Jones, M. Semsarilar, P. Wyman, M. Boerakker and S. P. Armes, Addition of water to an alcoholic RAFT PISA formulation leads to faster kinetics but limits the evolution of copolymer morphology, *Polym. Chem.*, 2016, **7**, 851–859.

36 G. Desnos, A. Rubio, C. Gomri, M. Gravelle, V. Ladmiral and M. Semsarilar, Semi-fluorinated di and triblock copolymer nano-objects prepared via RAFT alcoholic dispersion polymerization (PISA), *Polymers*, 2021, **13**, 2502–2515.

37 M. J. Derry, L. A. Fielding and S. P. Armes, Industrially-relevant polymerization-induced self-assembly formulations in non-polar solvents: RAFT dispersion polymerization of benzyl methacrylate, *Polym. Chem.*, 2015, **6**, 3054–3062.

38 L. A. Fielding, M. J. Derry, V. Ladmiral, J. Rosselgong, A. M. Rodrigues, L. P. D. Ratcliffe, S. Sugihara and S. P. Armes, RAFT dispersion polymerization in non-polar solvents: facile production of block copolymer spheres, worms and vesicles in n-alkanes, *Chem. Sci.*, 2013, **4**, 2081–2087.

39 L. Houillot, C. Bui, M. Save, B. Charleux, C. Farcet, C. Moire, J. A. Raust and I. Rodriguez, Synthesis of well-defined polyacrylate particle dispersions in organic medium using simultaneous RAFT polymerization and self-assembly of block copolymers. A strong influence of the selected thiocarbonylthio chain transfer agent, *Macromolecules*, 2007, **40**, 6500–6509.

40 Y. Pei, L. Thurairajah, O. R. Sugita and A. B. Lowe, RAFT dispersion polymerization in nonpolar media: polymeriz-

ation of 3-phenylpropyl methacrylate in n-tetradecane with poly(stearyl methacrylate) homopolymers as macro chain transfer agents, *Macromolecules*, 2015, **48**, 236–244.

41 C. György and S. P. Armes, Recent advances in polymerization-induced self-assembly (PISA) syntheses in non-polar media, *Angew. Chem., Int. Ed.*, 2023, **62**, e202308372.

42 C. Grazon, P. Salas-Ambrosio, E. Ibarboure, A. Buol, E. Garanger, M. W. Grinstaff, S. Lecommandoux and C. Bonduelle, Aqueous ring–opening polymerization–induced self–assembly (ROPISA) of N–carboxyanhydrides, *Angew. Chem., Int. Ed.*, 2020, **59**, 622–626.

43 C. Grazon, P. Slalas-Ambrosio, S. Antoine, E. Ibarboure, O. Sandre, A. J. Clulow, B. J. Boyd, M. W. Grinstaff, S. Lecommandoux and C. Bonduelle, Aqueous ROPISA of α-amino acid N-carboxyanhydrides: polypeptide block secondary structure controls nanoparticle shape anisotropy, *Polym. Chem.*, 2021, **12**, 6242–6251.

44 A. H. Morrell, N. J. Warren and P. D. Thornton, The production of polysarcosine-containing nanoparticles by ring-opening polymerization-induced self-assembly, *Macromol. Rapid Commun.*, 2024, **45**, 2400103.

45 E. Tinajero-Díaz, N. Judge, B. Li, T. Leigh, R. D. Murphy, P. D. Topham, M. J. Derry and A. Heise, Poly(l-proline)-stabilized polypeptide nanostructures via ring-opening polymerization-induced self-assembly (ROPISA), *ACS Macro Lett.*, 2024, **13**, 1031–1036.

46 M. A. H. Farmer, O. M. Musa and S. P. Armes, Efficient synthesis of hydrolytically degradable block copolymer nanoparticles via reverse sequence polymerization–induced self–assembly in aqueous media, *Angew. Chem., Int. Ed.*, 2023, **62**, e20230952.

47 M. A. H. Farmer, O. M. Musa and S. P. Armes, Combining crystallization-driven self-assembly with reverse sequence polymerization-induced self-assembly enables the efficient synthesis of hydrolytically degradable anisotropic block copolymer nano-objects directly in concentrated aqueous media, *J. Am. Chem. Soc.*, 2024, **146**, 16926–16934.

48 P. Chohan, C. György, O. O. Mykhaylyk, G. M. Prentice, S. V. Filip, M. J. Payne, G. Manna and S. P. Armes, RAFT Dispersion Polymerization of 2-Hydroxyethyl Methacrylate in Non-polar Media, *Macromolecules*, 2024, **57**, 11738–11752.

49 H. Li, R. M. Shakaroun, S. M. Guillaume and J.-F. Carpentier, Recent advances in metal-mediated stereoselective ring-opening polymerization of functional cyclic esters towards well-defined poly(hydroxy acid)s: from stereoselectivity to sequence-control, *Chem. – Eur. J.*, 2020, **26**, 128–138.

50 A. Dhaini, R. M. Shakaroun, A. Alaaeddine, J.-F. Carpentier and S. M. Guillaume, Metal-Catalyzed Stereoselective Ring-Opening Polymerization of Functional β-Lactones: Methylene-Alkoxy Fluorinated Polyhydroxyalkanoates Unveil the Role of Non-Covalent Interactions, *Polym. Chem.*, 2024, **15**, 999–1014.

51 H. Kakwere and S. Perrier, Design of complex polymeric architectures and nanostructured materials/hybrids by living radical polymerization of hydroxylated monomers, *Polym. Chem.*, 2011, **2**, 270–288.

52 L. Xu, F. Mallamace, Z. Yan, F. W. Starr, S. V. Buldyrev and H. Eugene Stanley, Appearance of a fractional Stokes–Einstein relation in water and a structural interpretation of its onset, *Nat. Phys.*, 2009, **5**, 565–569.

53 C. G. Jaffredo, J.-F. Carpentier and S. M. Guillaume, Controlled ROP of β-butyrolactone simply mediated by amidine, guanidine, and phosphazene organocatalysts, *Macromol. Rapid Commun.*, 2012, **33**, 1938–1944.

54 J.-F. Carpentier, Rare-earth complexes supported by tripodal tetradentate bis (phenolate) ligands: a privileged class of catalysts for ring-opening polymerization of cyclic esters, *Organometallics*, 2015, **34**, 4175–4189.

55 E. Themistou, G. Battaglia and S. P. Armes, Facile synthesis of thiol-functionalized amphiphilic polylactide–methacrylic diblock copolymers, *Polym. Chem.*, 2014, **5**, 1405–1417.

56 K. Skrabania, A. Miasnikova, A. M. Bivigou-Koumba, D. Zehm and A. Laschewsky, Examining the UV-vis absorption of RAFT chain transfer agents and their use for polymer analysis, *Polym. Chem.*, 2011, **2**, 2074–2083.

57 J. V. M. Weaver, I. Bannister, K. L. Robinson, X. Bories-Azeau, S. P. Armes, M. Smallridge and P. McKenna, Stimulus-responsive water-soluble polymers based on 2-hydroxyethyl methacrylate, *Macromolecules*, 2004, **37**, 2395–2403.

58 T. Gruendling, R. Pickford, M. Guilhaus and C. Barner-Kowollik, Degradation of RAFT polymers in a cyclic ether studied via high resolution ESI-MS: Implications for synthesis, storage, and end-group modification, *J. Polym. Sci., Part A:Polym. Chem.*, 2008, **46**, 7447–7461.

59 K. Liang and R. A. Hutchinson, Solvent effects in semi-batch free radical copolymerization of 2-hydroxyethyl methacrylate and styrene at high temperatures, *Macromol. Symp.*, 2013, **325–326**, 203–212.

60 K. Liang, T. R. Rooney and R. A. Hutchinson, Solvent effects on kinetics of 2-hydroxyethyl methacrylate semi-batch radical copolymerization, *Ind. Eng. Chem. Res.*, 2014, **53**, 7296–7304.

61 S. Bhattacharjee, DLS and zeta potential – What they are and what they are not?, *J. Controlled Release*, 2016, **235**, 337–351.

62 P. A. Montaño-González, L. M. Bravo-Lozano, S. Chevance, F. Dole, J. Rosselgong, P. Loyer, S. Tranchimand, J.-P. Chapel, F. Gauffre, C. Schatz and L. M. Bravo-Anaya, Interactions between PEI and biological polyanions and the ability of glycosaminoglycans in destabilizing PEI/peGFP-C3 polyplexes for genetic material release, *Int. J. Biol. Macromol.*, 2025, **301**, 14035.

63 E. E. Brotherton, F. L. Hatton, A. A. Cockram, M. J. Derry, A. Czajka, E. J. Cornel, P. D. Topham, O. O. Mykhaylyk and S. P. Armes, In situ SAXS studies during RAFT aqueous emulsion polymerization, *J. Am. Chem. Soc.*, 2019, **141**, 13664–13675.

64 A. Guinier, G. Fournet and K. L. Yudowitch, *Small-Angle Scattering of X-Rays*, 1955.